Optimized high performance thermoelectric generator with combined segmented and asymmetrical legs under pulsed heat input power

Samson Shittu[a]

Guiqiang Li[a, *]

Guiqiang.Li@hull.ac.uk

Xudong Zhao[a]

Xiaoli Ma[a]

Yousef Golizadeh Akhlaghi[a]

Emmanuel Ayodele[b]

[a]School of Engineering and Computer Science, University of Hull, HU6 7RX, UK

[b]Institute of Robotics, Autonomous Systems and Sensing, University of Leeds, LS2 9JT, UK

[*]Corresponding author. School of Engineering and Computer Science, University of Hull, Hull, HU6 7RX, UK.

Abstract

In this study, a segmented asymmetrical thermoelectric generator (SASTEG) is numerically investigated to optimize its electrical performance and mechanical reliability under transient and steady state conditions. The thermal and electrical performance of the SASTEG and TEG under transient and steady state heating conditions are studied and compared. A three-dimensional numerical model is developed and solved using finite element method in COMSOL 5.3 Multiphysics software. Temperature dependent thermoelectric material properties are considered, and the elastoplastic behaviour of copper and solder is accounted for in the thermal stress analysis. The initial SASTEG geometry used in this study is subsequently optimized to reduce the maximum von Mises stress developed in its legs while maintaining its enhanced power output. Results obtained show that the optimized SASTEG provided a power output enhancement of 117.11% compared to that of the conventional TEG under rectangular pulsed heat condition. Also, the asymmetrical leg geometry used in the SASTEG n-type leg provided a reduced thermal stress of 39.21% in the lower segment (cold side) compared to the symmetrical leg geometry used in the p-type leg lower segment. This study will provide vital guidance in the design of high-performance TEG with improved mechanical reliability.

Keywords: Pulsed heat power; Segmented thermoelectric generator; Asymmetrical leg; Thermal stress; Performance enhancement

1 Introduction

Preventing a world energy crisis is one of the most important tasks of the 21st century due to the significant rate at which the world's energy demand is growing because of population growth and industrialization [1]. In addition, the excessive use of the depleting fossil fuels has caused global warming and environmental pollution thus, a viable solution is to promote the use of renewable and clean energy [2,3]. Renewable energy sources offer several advantages such as; sustainability, low pollution and economic benefits. Therefore, an increased amount of research on the development and application of renewable energy sources is being carried out as a solution to reduce the over reliance on fossil fuels [4,5].

Thermoelectric (TE) device is a viable clean energy solution that can convert thermal energy into electrical energy when a temperature gradient is present via the Seebeck effect. While a reverse phenomenon called Peltier effect enables the TE device to generate thermal energy from electrical energy [6]. A thermoelectric generator (TEG) can be used to convert waste heat into electricity thereby, reducing the use of fossil fuel. Compared with other waste heat recovery technologies, thermoelectric generators offer several advantages including gas free emissions, solid-state operation, no noise, maintenance free operation, no moving parts, vast scalability, long periods of reliable operation and zero environmental pollution [7,8]. These unique advantages have increased the application of TEG for power generation in space and military applications [9], wearable sensors [10–13], waste heat recovery [14–18], wireless sensor network [19,20], micro-cogeneration [21] and marine engine application [22].

However, the wider application of thermoelectric generator is still limited due to its low energy conversion efficiency and corresponding high material cost. Therefore, the main focus of TEG research has been to achieve a high energy conversion efficiency at a reduced cost [23]. This can be achieved by optimization of the thermoelectric materials and thermoelectric generator geometry. A dimensionless parameter known as thermoelectric material figure of merit ($Z = \frac{\alpha^2}{\kappa \cdot R}$) is usually used to determine the performance of a thermoelectric material, where α is the Seebeck coefficient, κ is thermal conductivity and R is electrical resistivity [24]. Generally, thermoelectric materials with high electrical conductivity (σ), low thermal conductivity and high Seebeck coefficient are desirable to increase the thermoelectric figure of merit and subsequently enhance the performance of the thermoelectric generator [25]. However, the improvement of all three thermoelectric parameters (α, κ and σ) simultaneously is the general challenge in thermoelectric because these quantities are interrelated to each other by the charge carrier concentration (n) [26].

Optimizing the geometry of a thermoelectric generator is a way to enhance its efficiency and power output [27]. Ferreira-Teixeira et al. [28] performed numerical simulations using finite element method to optimize the geometry of a thermoelectric generator. Two geometries of the thermoelectric legs were studied including cubic and cylindrical geometries using COMSOL software. Results obtained showed that there exists an optimal ratio between the height and width of the thermoelectric legs which enhances the performance of the TEG and increasing the cross-sectional area of the legs could enhance the power produced by the TEG. Finite element method was also used by Shittu et al. [29] to optimize the geometry of a thermoelectric generator attached to a Photovoltaic module. Using COMSOL simulation software, they found that the optimum thermoelectric geometry in a hybrid Photovoltaic-thermoelectric (PV-TE) device is different from that in a stand-alone TEG.

The use of two different thermoelectric materials to form a segmented thermoelectric generator (STEG) is advantageous because no single material is thermally stable within the entire temperature regime and a higher overall performance can be obtained if two thermoelectric materials with high figure of merit are utilized in their optimum temperature region [30]. Ge et al. [31] presented a general method to optimize the structure and load current of a segmented thermoelectric generator. Bismuth telluride and Skutterudite were used as the cold and hot side thermoelectric materials and finite element method was utilized for the simulation. They found that there is an optimal ratio of hot and cold side materials to obtain maximum power output in a segmented thermoelectric generator. Recently, Lundgaard et al. [32] presented a new design of segmented off-diagonal thermoelectric generators using density-based topology optimization to optimize the off-diagonal figure-of-merit and off-diagonal electric power output of the thermoelectric generations. They found that using the proposed optimization method, the off-diagonal figure-of-merit and the off-diagonal electrical power output could be improved by 233% and 229% respectively compared to other optimization methods currently available.

Furthermore, Ouyang et al. [33] demonstrated the commercial feasibility and competitiveness of segmented thermoelectric generators. They argued that proper segmentation of TEG using materials with high figure of merit can offer <1$/W cost-performance ratio. Fan et al. [34] studied the thermoelectric and mechanical performance of an annular thermoelectric generator and they found that increasing the thermoelectric leg would reduce the electrical performance but improve the mechanical reliability of the annular TEG. Ming et al. [35] performed a numerical analysis of a segmented thermoelectric generator and the thermal stress developed was studied. Temperature gradient induced thermal stress was studied with several heat flux distributions and they found that the thermal stress developed in the horizontal direction is the major cause of failure or damage in the STEG.

Al-Merbati et al. [36] studied the influence of thermoelectric leg geometry on the thermal efficiency and thermal stress developed in the TEG. They found that the use of thermoelectric legs with asymmetrical geometry (trapezoidal shape) can reduce the maximum thermal stress developed in the thermoelectric leg thus, increasing the life-span of the device. Fabián-Mijangos et al. [37] presented an experimental study of a thermoelectric generator with asymmetrical legs. Results obtained showed that the thermoelectric figure of merit of the TEG with asymmetrical legs was also double that of the TEG with conventional square legs thus, the TEG with asymmetrical legs performed better than the conventional TEG. Recently, Liu et al. [38] presented a new design of solar TEG with combination of segmented materials and asymmetrical legs with variable cross-sectional area long the leg length. A three-dimensional numerical model was used to optimize the solar thermoelectric generator and the optimum leg length ratio of the two segmented materials and the optimum cross-sectional area ratio of the TEG cold and hot ends were presented. Results obtained showed that the segmented design increased the power output by 14.9% and 16.6% respectively compared to two different non-segmented design when the leg length was optimized. A further enhancement was observed when asymmetrical legs were introduced to the segmented design and the power output increased by 4.21% compared to the optimal segmented design.

The application of transient and pulsed heat inputs is another method to enhance the performance of thermoelectric devices. Mahmoudinezhad et al. [39] presented an experimental and numerical study on the transient response of an oxide thermoelectric generator to variation of solar radiation in semi-cloudy weather. Results showed that the graphite absorber attached to the hot surface of the solar TEG enhanced the power generation performance of the TEG due to increased absorbed radiation. Similarly, an experimental and numerical study on the behaviour of thermoelectric generators exposed to transient heat sources was performed by Nguyen et al. [40]. Open-circuit and closed-circuit experiments were performed, and results showed that it is imperative to consider the Thomson effect in TEG analysis for accurately predicting the thermoelectric generator performance. Recently, Merienne et al. [41] performed an experimental study on the effects of thermal cycling and heating rate on the power generation performance of thermoelectric generators over time. Three TEGs of the same specifications were subjected to different heating rates and results showed that all the TEGs had a significant performance reduction after just 600 cycles.

Chen et al. [42] presented a numerical analysis of the power output and efficiency of a thermoelectric generator operated under a controlled temperature. Results obtained showed that the average power output and efficiency of the TEG could be significantly enhanced by the oscillation of temperature. Furthermore, Chen et al. [43] performed a very significant study on the effect of pulsed heat power on thermoelectric generator's thermal and electrical

performances. A numerical and experimental study was performed and the advantage of pulsed heat power over alternating temperature gradient was presented. Results obtained showed that pulsed heat power enhanced the performance of TEG (in terms of maximum efficiency) by 8.6 times that of the alternating temperature gradient under the same input power condition. In addition, they found that the application of transient rectangular pulsed heat power resulted in a higher power output compared to the steady state. Recently, Asaadi et al. [44] performed a similar study on the effect of pulsed heat power with different types of input functions on the thermal and electrical performance of an annular thermoelectric generator. Results obtained showed that the transient pulsed heating improved the efficiency of the annular TEG for all types of heat input functions and rectangular input function provided better improvements compared to other functions. In fact, when a duty cycle of 0.1 and ratio of maximum heat flux to minimum heat flux (b/a = 48), the rectangular input function provided a maximum efficiency enhancement of 249.36%. The additional literature reviewed are shown in Table 1 alongside their key conclusions concisely stated.

Table 1 Additional literature reviewed.

alt-text: Table 1

Reference	Research area	Key conclusion
Ma et al. [54]	TEG geometry optimization	There exists an optimal electric conducting plate thickness for obtaining maximum power output
Li et al. [55]	TEG geometry optimization	Thermoelectric leg length and area significantly affects the performance of the hybrid PV-TE.
Sun et al. [56]	TEG geometry optimization	The optimization of the thermoelectric geometry is important to develop more compact and highly efficient thermoelectric generators.
Li et al. [57]	TEG load resistance	Optimum TE load resistance in a hybrid PV-TE should be lower than its internal resistance
Yu et al. [58]	TEG load resistance	The optimum load resistance to internal resistance ratio for obtaining enhanced thermoelectric generator power output was found to be 1.5–1.8
Li et al. [59]	Heat pipes with TEG	Use of micro-channel heat pipe in PV-TE can reduce quantity of TEG needed.
Li et al. [60]	Heat pipes with TEG	The use of solar concentrating thermoelectric generators in combination with micro-channel heat pipe can significantly reduce the cost of the system.
Li et al. [61]	Heat pipes with TEG	The solar concentration thermoelectric generators combined with micro-channel heat pipe array had a higher electrical efficiency and lower cost compared to traditional solar thermoelectric generators.
Li et al. [62]	Heat pipes with TEG	The novel micro-channel heat pipe evacuated tube solar collector incorporated thermoelectric generation had a high thermal performance with additional electricity production
Shu et al. [63]	Segmented TEG	The segmented thermoelectric generator maximum power was higher than that of the TEG by 13.4%.
Tian et al. [64]	Segmented TEG	The segmented TEG is better for high-temperature heat source and for large temperature differences compared to the non-segmented TEG.
Shen et al. [50]	Segmented annular TEG	Compared to the non-segmented annular thermoelectric generator, the segmented annular thermoelectric generator becomes clearly better and preferable as the temperature ratio increases.
Shittu et al. [49]	Segmented annular TEG	The segmented annular TEG provided an increased power output compared to the non-segmented annular TEG.
Yamashita et al. [65]	Transient study	The application of periodically alternating temperature gradient to the TEG can enhance the efficiency of the TEG
Yamashita et al. [66]	Transient study	The reason for the low efficiency of the TEG with alternating temperature gradient is because of the high external resistance and long period of rectangular wave of the input voltage applied across the two TEGs.

The extensive literature review carried out above shows the vital importance of optimizing the thermoelectric generator geometry, using segmented TEG, performing thermal stress analysis, using asymmetrical legs for TEG, using transient and pulsed heat power to enhance the performance of a thermoelectric generator. There is currently only one study [38] on a thermoelectric generator with combined segmented and asymmetrical legs (varying cross-sectional area across leg length) however, only steady state heating was considered and the focus was on optimizing the electrical performance of the TEG. Furthermore, there are currently only two studies [43,44] on the effect of pulsed heat power on thermoelectric generators however, both studies did not present the analysis of thermal stress developed in the TEG. In addition, temperature dependent thermoelectric material properties were not considered in Ref. [43] while the study carried out in Ref. [44] was specifically for annular thermoelectric generators. Therefore, this study is very vital as it seeks fill in the research gaps.

For the first time, the optimization of a thermoelectric generator by the application of pulsed heat power to a TEG with combined segmented and asymmetrical legs is presented in this study. In addition, the thermal stress developed in the TEG is analysed and this stress is reduced by optimizing the geometry of the TEG. While many previous studies have focussed solely on optimizing the electrical performance of the TEG with no consideration for the thermal stress developed, this study places emphasis on enhancing the electrical performance of the TEG and simultaneously reducing the thermal stress developed so as to increase the life span of the device. Furthermore, transient rectangular pulsed heat power and steady state heating are applied to the thermoelectric generator. This study investigates the thermal (temperature and thermal stress) and electrical (voltage, current, power output) performance of a segmented asymmetrical thermoelectric generator (SASTEG) under both transient and steady state heating condition and a performance comparison with a conventional thermoelectric generator (TEG) is presented. Finite element method is used to perform the numerical analysis, COMSOL 5.3 Multiphysics software is employed and temperature dependent thermoelectric material properties are considered to ensure the accuracy of the numerical study. The remainder of this paper is organized as follows; Section 2 provides the geometry description, Section 3 presents the numerical model, Section 4 presents the results obtained and discussion while Section 5 provides the conclusions drawn from this study.

2 Geometry description and material selection

The geometry of a typical thermoelectric generator (TEG) is shown in Fig. 1a while that of the segmented asymmetrical thermoelectric generator (SASTEG) is shown in Fig. 1b. The optimized geometry of the SASTEG is shown in Fig. 1c and the rectangular heat flux pulse applied to the hot side of the TEG and SASTEG is shown in Fig. 1d. A typical thermoelectric generator consists of alumina ceramic which enables thermal conductivity and electrical insulation, copper conductors which connects the semiconductor materials and facilitates electrical conductivity within the generator, solder material which is useful for reducing thermal stress developed in the TEG and a pair of n-type and p-type semiconductor legs. An electric closed circuit is formed when an external load resistor (R_L) is connected across the copper terminals of the TEG thus power output of the TEG can be measured. Transient and steady state heating conditions are applied to the hot side of the TEG and SASTEG while the cold side is maintained at a constant temperature. In the case of the SASTEG, two different thermoelectric material are used for the p-type leg as shown in Fig. 1b. The dimensions of the TEG and SASTEG are exactly the same so as to ensure accurate comparison of performance. The total height of the thermoelectric legs remains the same in both the TEG and SASTEG therefore,

$$H = H_1 + H_2 = H_3 + H_4 \quad (1)$$

where H_1 is the height of the hot segment p-type thermoelectric material, H_2 is that of the cold segment p-type material, H_3 is the height of the hot segment n-type thermoelectric material and H_4 is that of the cold segment n-type material.

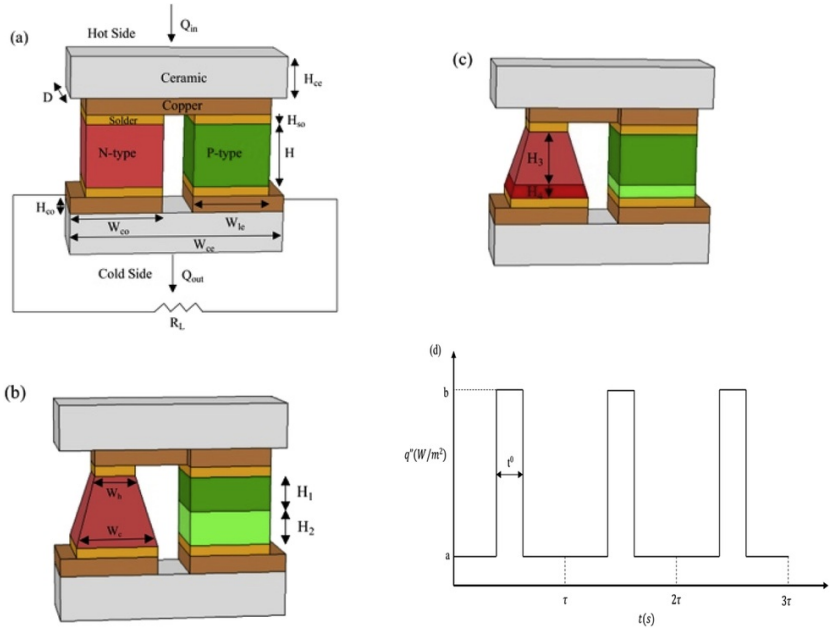

Fig. 1 Schematic diagram of (a) thermoelectric generator (b) segmented asymmetrical thermoelectric generator and (c) optimized SASTEG geometry (d) rectangular heat flux pulse.

alt-text: Fig. 1

For the sake of simplicity, the n-type and p-type thermoelectric legs are of the same dimensions. In this study, only the n-type leg is asymmetrical because the n-type materials are universally weaker compared to their p-type counterparts [45]. In addition, asymmetrical legs have been reported to perform better than the rectangular legs [37]. Therefore, to improve the performance of the n-type leg and consequently optimize the SASTEG performance, the n-type leg is made asymmetrical. The effect of asymmetrical p-type leg is beyond the scope of this present study and would be considered in future works. The asymmetrical n-type leg used in the SASTEG is achieved by varying the cross-sectional area across the leg height. Again, to simplify the analysis, the hot side cross-sectional area of the asymmetrical leg is half of that of the cold side therefore,

$$W_{le} = W_c = W_h \times 2 \quad \textbf{(2)}$$

where W_{le} is the width of the leg, W_h is the width of the hot side n-type asymmetrical thermoelectric leg and W_c is that of the cold side thermoelectric leg. This ratio is kept constant throughout the study. However, the height ratio of the segmented thermoelectric materials is varied to find the optimum value. Thus,

$$H_p = \frac{H_1}{H_2} \quad \textbf{(3)}$$

$$H_n = \frac{H_3}{H_4} \quad \textbf{(4)}$$

where H_p is height ratio of the SASTEG p-type material and H_n is that of the n-type materials.

The geometric dimensions of the thermoelectric generator are shown in Table 2. Considering the optimum operating temperature range of thermoelectric materials, Bismuth telluride (Bi_2Te_3) and Skutterudite ($CoSb_3$) have been chosen for the cold segment/side and hot segment/side of the SASTEG respectively. While for the TEG, only Skutterudite thermoelectric material is used so as to ensure accurate comparison can be made with the SASTEG in the high temperature conditions under which both systems are studied. Generally, the TEG's performance is significantly affected by the choice of materials used. Thermoelectric materials can be divided into three main temperature ranges: low temperature <500K (e.g. Bi_2Te_3), middle temperature 500–900K (e.g. PbTe, $CoSb_3$) and high temperature >900K (e.g. SiGe) [46]. Bismuth telluride is the best material for the low temperature range because of its high figure of merit thus it is used in this study while the Skutterudite's figure of merit increases with increasing temperature therefore, it is appropriate for this kind of study in which pulsed heat power is applied, and high temperature is achieved. In addition, both Bi_2Te_3 and $CoSb_3$ have strong mechanical properties and provide good electrical performance. Temperature dependent thermoelectric material properties are used in this study to ensure result accuracy and are fitted into polynomials with temperature shown in Table 3.

Table 2 Geometric dimensions of thermoelectric generator [43].

alt-text: Table 2

Parameter	Symbol	Value
Ceramic height	H_{ce}	0.75 mm
Solder height	H_{so}	0.175 mm
Copper height	H_{co}	0.3 mm
Leg height	H	1.15 mm
Ceramic depth	D	1.4 mm
Ceramic width	W_{ce}	3.92 mm
Leg width	W_{le}	1.4 mm
Copper width	W_{co}	1.68 mm

Table 3 Temperature dependent thermoelectric material properties [50].

alt-text: Table 3

Material equations
Thermal conductivity

$k_{nh}(T) = 6.943541 - 2.486028 \times 10^{-2} T + 9.749004 \times 10^{5} T^2 - 2.532973 \times 10^{-7} T^3 + 3.938164 \times 10^{-10} T^4$
$k_{ph}(T) = 1.003769 \times 10^{1} + 1.569560 \times 10^{-1} T - 8.040513 \times 10^{-4} T^2 + 2.155576 \times 10^{-6} T^3 - 3.177501 \times 10^{-9} T^4 + 2.436340 \times 10^{-12} T^5 - 7.572115 \times 10^{-16} T^6$
$k_{pc}(T) = 1.151451 \times 10^{-1} + 4.474949 \times 10^{-2} T - 2.597266 \times 10^{-4} T^2 + 5.558334 \times 10^{-7} T^3 - 3.676412 \times 10^{-10} T^4$
$k_{nc}(T) = 9.550516 - 5.393685 \times 10^{-2} T + 1.123143 \times 10^{-4} T^2 - 6.666667 \times 10^{-8} T^3$
Electrical resistivity
$\rho_{pc}(T) = 2.728214 \times 10^{-5} - 2.254395 \times 10^{-7} T + 7.275808 \times 10^{-10} T^2 - 6.25084 \times 10^{-13} T^3$
$\rho_{nc}(T) = 1.167186 \times 10^{-5} - 9.313746 \times 10^{-8} T + 3.786254 \times 10^{-10} T^2 - 3.582737 \times 10^{-13} T^3$
$\rho_{ph}(T) = 3.445724 \times 10^{-6} + 3.427092 \times 10^{-9} T + 4.683604 \times 10^{-12} T^2 - 3.534736 \times 10^{-15} T^3$
$\rho_{nh}(T) = 1.814895 \times 10^{-6} + 5.429077 \times 10^{-9} T + 1.743566 \times 10^{-12} T^2 - 2.665253 \times 10^{-15} T^3$
Seebeck coefficient
$\alpha_{pc}(T) = 1.4831 \times 10^{-3} - 1.3905 \times 10^{-5} T + 5.3964 \times 10^{-8} T^2 - 8.8088 \times 10^{-11} T^3 + 5.0618 \times 10^{-14} T^4$
$\alpha_{ph}(T) = 9.8267 \times 10^{-5} + 1.4455 \times 10^{-6} T - 4.8488 \times 10^{-9} T^2 + 9.2428 \times 10^{-12} T^3 - 8.6346 \times 10^{-15} T^4 + 3.0656 \times 10^{-18} T^5$
$\alpha_{nh}(T) = 1.9164 \times 10^{-4} - 3.4758 \times 10^{-6} T + 1.7756 \times 10^{-8} T^2 - 4.9992 \times 10^{-11} T^3 + 7.7054 \times 10^{-14} T^4 - 6.1429 \times 10^{-17} T^5 + 1.9864 \times 10^{-20} T^6$
$\alpha_{nc}(T) = 1.5178 \times 10^{-2} + 1.7621 \times 10^{-4} T - 8.1434 \times 10^{-7} T^2 + 1.8488 \times 10^{-9} T^3 - 2.0649 \times 10^{-12} T^4 + 9.0988 \times 10^{-16} T^5$

Where k_{nh} and k_{ph} are the thermal conductivities of n-type and p-type $CoSb_3$ respectively. k_{pc} and k_{nc} are the thermal conductivities of p-type and n-type Bi_2Te_3 respectively. ρ_{pc} and ρ_{nc} are the electrical resistivities of p-type and n-type Bi_2Te_3 respectively. ρ_{ph} and ρ_{nh} are the electrical resistivities of p-type and n-type $CoSb_3$ respectively. α_{pc} and α_{nc} are the Seebeck coefficients of p-type and n-type Bi_2Te_3 respectively. α_{ph} and α_{nh} are the Seebeck coefficients of p-type and n-type $CoSb_3$ respectively.

The remaining material properties are shown in Table 4. For the thermal stress analysis, ceramic and thermoelectric materials (Bi_2Te_3 and $CoSb_3$) are considered as brittle materials and the yield stress of Bi_2Te_3 is 112Mpa [36] and the ideal strength of $CoSb_3$ is 14.1 GPa [47]. Copper and solder are considered as elastoplastic materials, the yield stress and tangential modulus of copper are 70 MPa and 24 GPa respectively while those of solder are 26 MPa and 8.9 GPa respectively [34].

Table 4 Remaining material properties used in simulation [34,36,43,47,51–53].

alt-text: Table 4

Materials	Thermal conductivity, $\kappa\left(\frac{W}{m \cdot K}\right)$	Electrical conductivity, $\sigma\left(\frac{S}{m}\right)$	Specific heat capacity, $C_p\left(\frac{J}{kg \cdot K}\right)$	Density, $\rho_d\left(\frac{kg}{m^3}\right)$	Coefficient of thermal expansion, $\left(\frac{1}{K}\right)$	Young's Modulus, E (GPa)	Poisson's ratio	Seebeck coefficient, α (V/K)
Ceramic	25	1e-12	800	3970	0.68e-5	340	0.22	0
Copper	385	5.9e7	386	8930	1.7e-5	120	0.3	6.5e-6
Solder	55	2e7	210	7240	2.7e-5	44.5	0.33	0
Bi_2Te_3	–	–	154.4	7740	0.8e-5 ~ 1.32e-5	65–59	0.23	–
$CoSb_3$	–	–	238.7	7582	6.36e-6	145.38	0.223	–

3 Numerical model

Thermoelectric and thermal stress analyses are carried out in this study on both the segmented asymmetrical thermoelectric generator (SASTEG) and the conventional TEG.

3.1 Thermoelectric governing equations

The thermoelectric analysis includes the Peltier effect, Fourier effect, Joule effect and Thomson effect. Finite element method is utilized to solve the thermoelectric governing equations using COMSOL 5.3 Multiphysics software.

The thermoelectric effect can be described using coupled equation of heat transfer and current density continuity which are expressed as follows [43]:

Conversion of heat energy:

$$\rho_d C_p \frac{\partial T}{\partial t} + \nabla \cdot q'' = Q' \tag{5}$$

Continuity of electric current:

$$\nabla \cdot J = \frac{\partial \rho_c}{\partial t} \tag{6}$$

where C_p is specific heat capacity, ρ_d is density t is time, T is temperature, ρ_c is charge density, Q' is Joule heating energy and q'' is the input heat flux.

$$Q' = J \cdot E \tag{7}$$

$$q'' = -k\nabla \mathrm{T} + P'J \tag{8}$$

where P' is the Peltier coefficient and J is the electric current flux.

$$P' = ST \tag{9}$$

$$\mathrm{J} = -\sigma\nabla \mathrm{V} - \sigma\alpha\nabla \mathrm{T}$$

where σ is the electrical conductivity, k is thermal conductivity, V is electric scalar potential and α is the Seebeck coefficient. (10)

Substituting Eq. (7) and Eq. (8) into Eq. (5) and Eq. (6);

$$\rho_d C_p \frac{\partial T}{\partial t} + \nabla \cdot (-k\nabla \mathrm{T} + \alpha T(-\sigma\nabla \mathrm{V} - \sigma\alpha\nabla \mathrm{T})) = (-\sigma\nabla \mathrm{V} - \sigma\alpha\nabla \mathrm{T})(-\nabla \mathrm{V}) \tag{11}$$

$$-\sigma\left(\nabla^2 \mathrm{V} + \alpha\nabla^2 T\right) = \frac{\partial \rho_c}{\partial t} \tag{12}$$

The above equations can be used for both the steady state heating condition and the transient heating condition however, for the steady state heating condition,

$$\frac{\partial \rho_c}{\partial t} = 0 \tag{13}$$

3.2 Electrical performance equations

Considering the Seebeck effect, when a temperature difference is present, an open circuit voltage is generated which is given as [43]:

$$V_{oc} = \alpha\Delta \mathrm{T} \tag{14}$$

where V_{oc} is the open circuit voltage, $\Delta \mathrm{T}$ is the temperature difference across the TEG and α is the Seebeck coefficient.

When an external load resistor is connected to the TEG, the power output is expressed as

$$P_{out} = \left(\frac{\alpha\Delta \mathrm{T}}{R_L + R_{in}}\right)^2 \times R_L \tag{15}$$

where R_L is the external load resistance and R_{in} is the TEG's internal resistance. Maximum power output can be obtained when $R_L = R_{in}$.

$$P_{out} = \frac{(\alpha \Delta T)^2}{4R_L} \tag{16}$$

Input power applied to the TEG hot side is given as

$$Q_{in} = q'' \times A \tag{17}$$

where q'' is the input heat flux and A is the TEG hot side surface area.

In this study, stead-state heating (SSH) and pulsed heating (PH) are applied to both the SASTEG and the TEG. Duty cycle and period time (τ) are used to characterize the pulsed heat flux. Duty cycle $\left(\frac{t^0}{\tau}\right)$ is defined as the ratio of heating time (t^0) to period time. Throughout the simulations, the overall heat input in the pulsed heating case is equal to that of the steady state heating case. Rectangular function is used to model the pulsed heat input flux and considering Fig. 1d, the input time-average heat flux for the rectangular function is given as [44]:

$$q'' = a + (b - a) \times \frac{t^0}{\tau} \tag{18}$$

where b/a is the ratio of maximum input heat flux to minimum input heat flux for a time period. Throughout this study, $b/a = 12$ and $q'' = 60 kW \cdot m^{-2}$.

Considering six continuous time periods $(6\tau = 720s)$, the transient heat input is given as

$$q'' = (b - a) \times f(t) + a \tag{19}$$

where $f(t)$ is the rectangular input function.

3.3 Thermal stress governing equations

Thermal stress is developed in a thermoelectric generator because of the uneven expansion of the TEG components and to describe the displacement-strain relation, the coupled thermal stress equations are given by Ref. [35]:

$$\bar{\varepsilon}_{xx} = \frac{\partial \bar{u}}{\partial \bar{x}}, \bar{\varepsilon}_{yy} = \frac{\partial \bar{v}}{\partial \bar{y}}, \bar{\varepsilon}_{zz} = \frac{\partial \bar{w}}{\partial \bar{z}} \tag{20}$$

$$\bar{\varepsilon}_{xy} = 0.5\left(\frac{\partial \bar{u}}{\partial \bar{y}} + \frac{\partial \bar{v}}{\partial \bar{x}}\right), \bar{\varepsilon}_{yz} = 0.5\left(\frac{\partial \bar{w}}{\partial \bar{y}} + \frac{\partial \bar{v}}{\partial \bar{z}}\right), \bar{\varepsilon}_{xz} = 0.5\left(\frac{\partial \bar{w}}{\partial \bar{x}} + \frac{\partial \bar{u}}{\partial \bar{z}}\right) \tag{21}$$

Expressing the stress-strain relation in a dimensionless form using a non-symmetrical Jacobian gives,

$$\begin{Bmatrix} \bar{\sigma}_{xx} \\ \bar{\sigma}_{yy} \\ \bar{\sigma}_{zz} \\ \bar{\sigma}_{yz} \\ \bar{\sigma}_{zx} \\ \bar{\sigma}_{xy} \end{Bmatrix} = \frac{\bar{E}}{(1+v)(1-2v)} \begin{bmatrix} 1-v & v & v & 0 & 0 & 0 \\ v & 1-v & v & 0 & 0 & 0 \\ v & v & 1-v & 0 & 0 & 0 \\ 0 & 0 & 0 & 1-2v & 0 & 0 \\ 0 & 0 & 0 & 0 & 1-2v & 0 \\ 0 & 0 & 0 & 0 & 0 & 1-2v \end{bmatrix} \times \begin{Bmatrix} \bar{\varepsilon}_{xx} \\ \bar{\varepsilon}_{yy} \\ \bar{\varepsilon}_{zz} \\ \bar{\varepsilon}_{yz} \\ \bar{\varepsilon}_{zx} \\ \bar{\varepsilon}_{xy} \end{Bmatrix} - \begin{Bmatrix} 1 \\ 1 \\ 1 \\ 0 \\ 0 \\ 0 \end{Bmatrix} \frac{\bar{\alpha}\overline{ET}}{1-2v} \tag{22}$$

The three-principal stress in a TEG are represented as σ_1, σ_2 and σ_3 respectively. The von Mises equivalent stress can be obtained from the fourth strength theory of mechanics of materials also known as the distortion of energy theory which describes the entire stresses in all three dimensions as,

$$\sigma = \sqrt{\frac{\left[(\sigma_1 - \sigma_2)^2 + (\sigma_2 - \sigma_3)^2 + (\sigma_3 - \sigma_1)^2\right]}{2}} \tag{23}$$

Finite element method is used to solve all the equations above which are already built into COMSOL Multiphysics software therefore, the electrical and thermal performance of the TEG can be obtained from the coupled equations above.

3.4 Boundary conditions and computation procedure

To simplify the analysis, some basic assumptions are made while still ensuring there is no significant deviation from the real conditions. These assumptions are:

1) The input heat flux is applied to the top surface (hot side) of the TEG with temperature T_h while the bottom surface (cold side) is maintained at a constant temperature (T_c) of 300K.

2) Adiabatic condition is assumed therefore, no heat losses from all the other surfaces.

3) The hot side of the TEG is constrained during the thermal stress analysis while other boundaries are free.

4) Anisotropic material properties are not considered.

5) The lower left copper electrode is grounded while the lower right copper electrode is connected to the external resistor circuit.

6) Electrical and thermal contact resistance are not considered.

This numerical study is carried out using COMSOL Multiphysics 5.3 software and the electrical and thermal performance of the segmented asymmetrical thermoelectric generator and conventional TEG are studied and compared. The heat transfer in solids, electric currents, electrical circuit and solid mechanics interfaces are used in the simulation software. All materials are considered as linear elastic material and the plasticity interface is used to model the elastoplastic behaviour of copper and solder. A rectangular function is used in conjunction with the analytical function to model the rectangular input heat flux and the period is 120s. To ensure the transient and periodic heating is accurately modelled, the events interface in COMSOL is used and two explicit events are used to model the switching on and off time of the pulse heat power.

3.5 Numerical model validation

Two kinds of validations are done to ensure the numerical model could be used to accurate predict the performance of the thermoelectric generators. Firstly, a mesh convergence test is carried out in COMSOL. A uniform structured mesh is built and three grid systems with total elements of 4715, 11545 and 42756 are tested and compared to study the grid independence of the model. The temperature and open circuit voltage obtained using these three grid systems are shown in Fig. 2a and Fig. 2b respectively. What is observed from both figures is that the values for the three grid systems are very similar therefore, to reduce computation time, the grid with 4715 elements is selected for all simulations. Secondly, the numerical model is validated using similar works available in the literature. Since pulsed heat power and thermal stress are the two main Multiphysics to be modelled, the simulations carried out by Asaadi et al. [44] and Yilbas et al. [48] are recreated. The simulations conditions are reset to the ones used by the authors and similar parameters are used. The temperature from rectangular pulse heat obtained in the previous study [44] and this present study is shown in Fig. 2c while the thermal stress result obtained in the previous study [48] and this present is shown in Fig. 2d. It is clear from both figures that the results are very similar thus, the numerical model in this study is validated and results obtained from this study are justifiable.

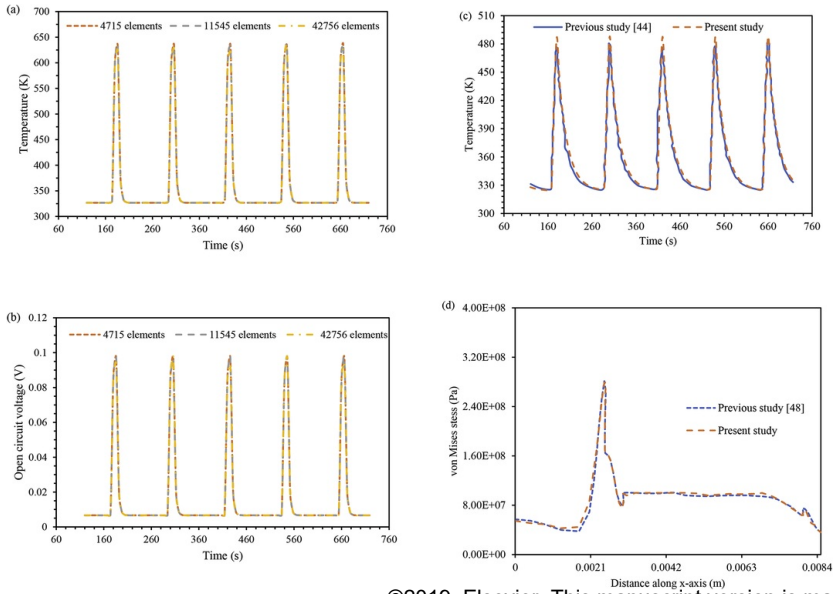

Fig. 2 Model validation (a) temperature and (b) open circuit voltage variation with time and mesh grid number (c) rectangular pulse validation with previous study [44] and (d) thermal stress validation with previous study [48].

alt-text: Fig. 2

4 Results and discussion

In this study, the thermal (temperature and thermal stress) and electrical (open circuit voltage, current and power output) performance of the segmented asymmetrical thermoelectric generator (SASTEG) is compared to that of the conventional thermoelectric generator (TEG). Transient rectangular pulsed heating and steady state heating are applied to both the SASTEG and TEG. Furthermore, the SASTEG is optimized to improve its power output and reduce the thermal stress developed in the device.

4.1 Thermal and electrical responses to pulsed heat flux

The responses of temperature, open circuit voltage, current and maximum power output of the SASTEG and TEG to transient rectangular pulsed heating and steady state heating for five continuous time periods are shown in Fig. 3a, Fig. 3b, c and d respectively. The steady state heating is represented by a straight line while the rectangular pulsed heating is represented by dotted and dashed lines for the SASTEG and TEG respectively. The spatially averaged heat flux used in all simulations is $60 kW{\cdot}m^{-2}$ and this is kept constant for both the pulsed heating and the steady state heating. Maximum power output can be obtained when the load resistance is matched to the TEG's internal resistance. Therefore, the external load resistance is varied till maximum power output is obtained which represents the matched load condition. The matched load under steady state heating for the SASTEG is found to be 0.012Ω and that of the TEG is found to be 0.006Ω. To simplify the analysis, the load resistance is kept constant throughout this study for both the steady state heating and the pulsed heating. Fig. 3a shows the spatially average temperature on the hot surface of the SASTEG and TEG while Fig. 3b shows the open circuit voltage obtained from both devices at steady state and pulsed heating conditions. It can be seen from Fig. 3 that the temperature voltage, current and power output follow the same trend and transient heating provides a better performance compared to steady state heating due to the fact that the rectangular pulsed heating allows for a greater temperature difference across the thermoelectric generator. Another clear observation from Fig. 3 is that the performance of the SASTEG is almost twice better than that of the TEG. This shows that the new design for thermoelectric generator incorporating the segmented materials and asymmetrical legs provides better electrical performance compared to the conventional TEG design.

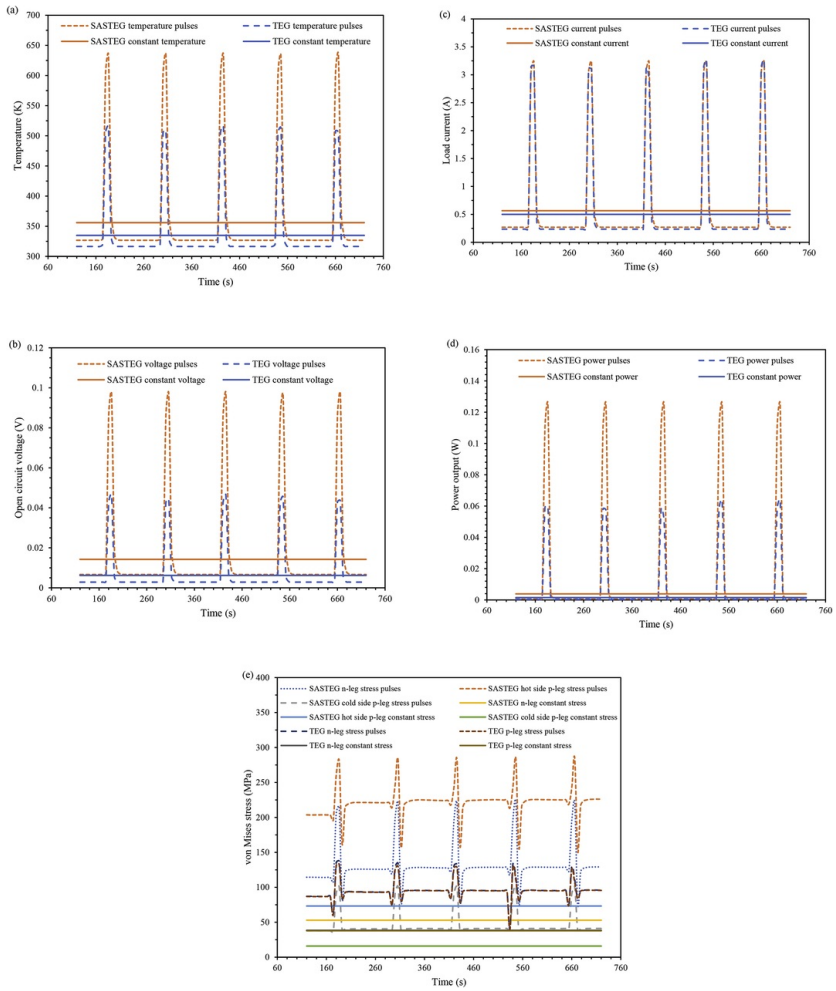

Fig. 3 Transient and steady state responses of the SASTEG and TEG (a) temperature (b) open circuit voltage (c) load current (d) power output and (e) von Mises stress.

alt-text: Fig. 3

The variation of the load current with time shown in Fig. 3c is identical for the SASTEG and TEG because of the difference in load resistance used to attain the maximum power output. The load current simply obeys the ohms law therefore, it is given as the output load voltage divided by the load resistance. Although, the load current in both the SASTEG and TEG is identical, the power output of each device is clearly different because of the difference in their open circuit voltage and corresponding output load voltage when the external resistance is matched. It can be seen from Fig. 3d that the maximum power output of the SASTEG at steady state condition is 0.0038469W while that of the TEG is 0.0015034W under the same condition. Therefore, a power output improvement of about 155.88% is observed under steady state condition simply by using the new design of the thermoelectric generator (i.e. SASTEG design). Furthermore, the application of transient rectangular pulsed heat power is shown in Fig. 3d to enhance the power output of the SASTEG and TEG significantly compared to the steady state heating. In fact, it can be seen that for the transient heating, the areas above the straight line (steady state heating) are larger than the areas below the straight line therefore, it can be concluded that the performance enhancement offered by the transient heating is significantly greater than that of the steady state heating. This finding is in agreement with [43,44].

The maximum von Mises stresses developed in the n-type and p-type thermoelectric legs of the SASTEG and TEG under transient and steady state heating conditions are shown in Fig. 3e. Although, the SASTEG offers a significant power enhancement compared to the TEG, it can be seen that the maximum von Mises stress developed in the legs of the SASTEG are greater than that of the TEG under both heating conditions. This is an expected trend

because the thermal stress developed is directly proportional to the temperature distribution in the TEG. Therefore, since the SASTEG operates at a significantly higher temperature compared to the TEG, its von Mises stress is expected to be higher. Also, it is obvious that the maximum von Mises stress under transient heating will be greater than that under the steady state heating due to the difference in operating temperature. The trend observed during the transient heating for the SASTEG and TEG shown in Fig. 3e is simply because of the periodic switching on and off of the pulse heat and this is why the von Mises stress goes to a minimum value and then it starts rising again as the rectangular pulse is applied. A solution to reduce the maximum von Mises stress developed in the SASTEG while maintaining its enhanced power output compared to the TEG is to optimize the SASTEG geometry.

4.2 Optimization of SASTEG

Two stages of optimization are carried out on the SASTEG including the p-type leg optimization and the n-type leg optimization. Firstly, the optimum height ratio for the segmented p-type leg (H_p) is found by varying this ratio for the range $0.2 \le H_p \le 0.5$. This range was considered because of the ease of manufacturing. If smaller ratios are considered like below 0.2, the material size for the low segment will be so small that it might be difficult to manufacture. In addition, since it might be difficult to consider all possible ratios that could be used, a sample range is chosen for analysis in this study. Fig. 4a shows the maximum von Mises stress developed in the hot and cold side legs of the p-type leg as the height ratio is varied. It is clear from Fig. 4a that the optimum height ratio for the segmented p-type leg (H_p) is 0.2. This is because, when $H_p = 0.2$, for all time periods and for both the hot side and cold side of the p-type leg, the von Mises stress developed is the lowest compared to other height ratios. Furthermore, as expected, the von Mises stress in the hot side p-type leg is greater than that of the cold side p-type leg due to the higher temperature impinged on the hot side. In addition, it is clear that the height ratio $H_p = 0.5$ provides the worst performance in terms of maximum von Mises stress developed thus, the need for the optimization of the initial geometry used in this study is shown. Fig. 4b shows the variation of the maximum von Mises stress in the SASTEG with the optimized p-type leg ($H_p = 0.2$) and it can be seen that compared to the thermal stress in the initial geometry shown in Fig. 3e, the maximum von Mises stress in the SASTEG hot side p-leg has been reduced by about 20.95% while that of the cold side p-leg has been reduced by about 21.16% due to the optimization of the height ratio under transient heating condition.

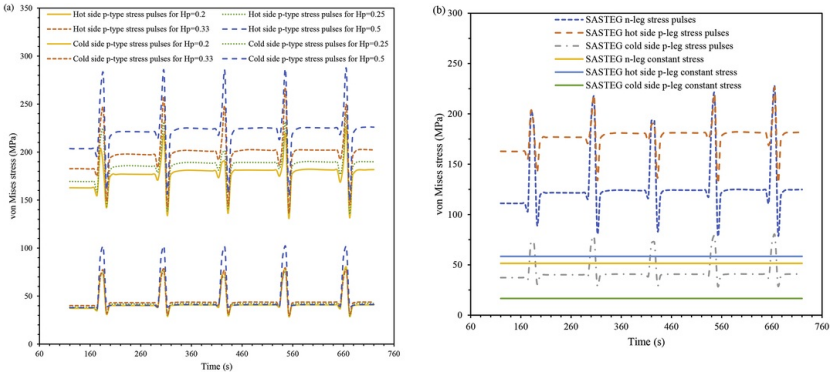

Fig. 4 (a) Variation of von Mises stress with SASTEG p-type height ratio (H_p) and (b) first optimized SASTEG p-type leg.

alt-text: Fig. 4

In the second optimization stage, the n-type leg of the SASTEG is optimized while keeping the p-type leg at the optimized height ratio ($H_p = 0.2$) obtained from the first optimization stage. Thus, the n-type leg is segmented similar to the p-type leg in the initial geometry then the optimum height ratio (H_n) for the newly segmented n-type leg is then found. Similar to the findings in Figs. 4a and 5a shows that the optimum height ratio for the n-type leg is also 0.2 and the worst height ratio is 0.5. Thus, the lowest von Mises stress can be obtained in the n-type segmented leg when the height ratio (H_n) of 0.2 is used. This again proves the benefit of geometry optimization of thermoelectric generators as lower von Mises stress means the life span of the TEG can be increased. Fig. 5b shows the variation of the maximum von Mises stress in the SASTEG with optimized p-type leg ($H_p = 0.2$) and optimized n-type leg ($H_n = 0.2$). It is clear that for both the hot side and the cold sides, the asymmetrical thermoelectric leg (n-type) possessed a lower von Mises stress compared to the symmetrical thermoelectric leg (p-type). In fact, the maximum von Mises stress in the hot side asymmetrical leg (n-type) is lower by about 7.45% compared to that of the symmetrical leg (p-type). While in the cold side, the maximum von Mises stress in the asymmetrical leg is lower by about 39.21% compared to that of the symmetrical leg. This finding clearly shows that the thermal stress in a thermoelectric generator can be reduced by the use of asymmetrical legs and this resonates well with the findings in Ref. [36].

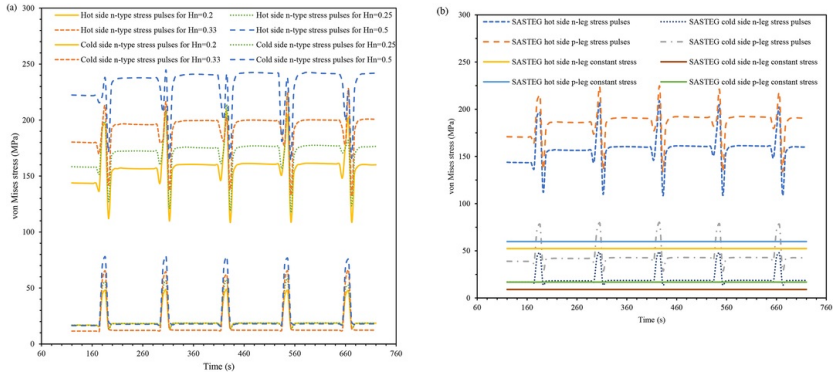

Fig. 5 (a) Variation of von Mises stress with SASTEG n-type height ratio (H_n) and (b) second stage optimized SASTEG.

alt-text: Fig. 5

Due to the results obtained from both optimization stages, the final optimized geometry in this study is found to be when $H_p = H_n = 0.2$. Thus, the power output of this optimized geometry compared to that of the conventional TEG. As shown in Fig. 6a, under transient response condition, the power output of the optimized SASTEG is greater than that of the conventional TEG by about 117.11%. This huge power output enhancement is obtained at a reduced thermal stress condition in the legs of the SASTEG thus, the device's reliability is improved. In addition, the three-dimensional temperature and voltage distribution in the optimized SASTEG is shown in Fig. 6b and c respectively.

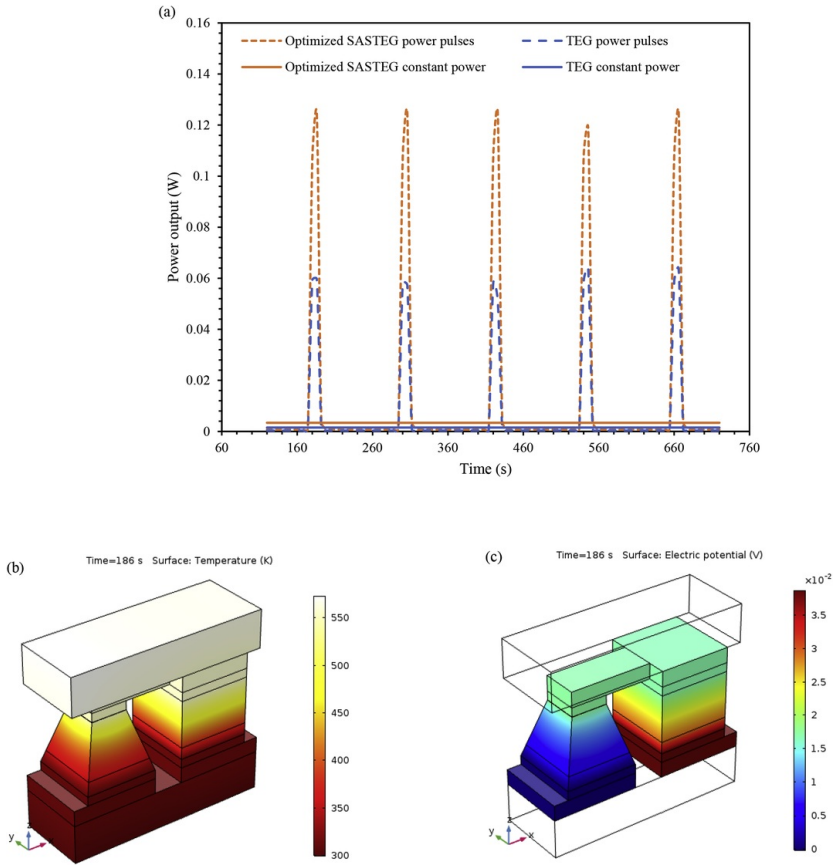

Fig. 6 Second stage optimized SASTEG (a) power output response comparison with TEG (b) three-dimensional temperature distribution and (c) voltage distribution.

alt-text: Fig. 6

4.3 Effect of duty cycle on optimized SASTEG and TEG performance

The duty cycle determines the ratio of the heating time to the period time thus, it is important to know the optimum value for the duty cycle at which the optimized SASTEG and the TEG can achieve the best performance. The duty cycle is varied from 0.1 to 0.5 and its effects on the maximum power output and maximum temperature on the hot surface of the SASTEG and TEG are shown in Fig. 7a and Fig. 7b respectively. It is obvious from both figures that as the duty cycle increases from 0.1 to 0.5, the power output and temperature of both the SASTEG and TEG reduces. Thus, the optimum duty cycle is 0.1 which is the initial value used throughout the study. The reason for the decrease in performance as the duty cycle increases is due to the fact that as shown in Eq. (18), the duty cycle also determines the maximum and minimum input heat flux applied to the devices. Thus, even though in this study, the heating time for peak heat flux is increased as the duty time increases (since period is constant and b/a is constant), the peak heat flux is reduced thus, the temperature difference across the device is reduced and consequently, the performance of both the SASTEG and TEG is reduced. Therefore, under the conditions used in this study, very short duty cycles are desirable as a decrease in duty cycle enhances the performance of the SASTEG and TEG because of the aforementioned reason. Also, Fig. 7a and b resonate the general findings throughout this study that the SASTEG provides an enhanced performance compared to the conventional TEG.

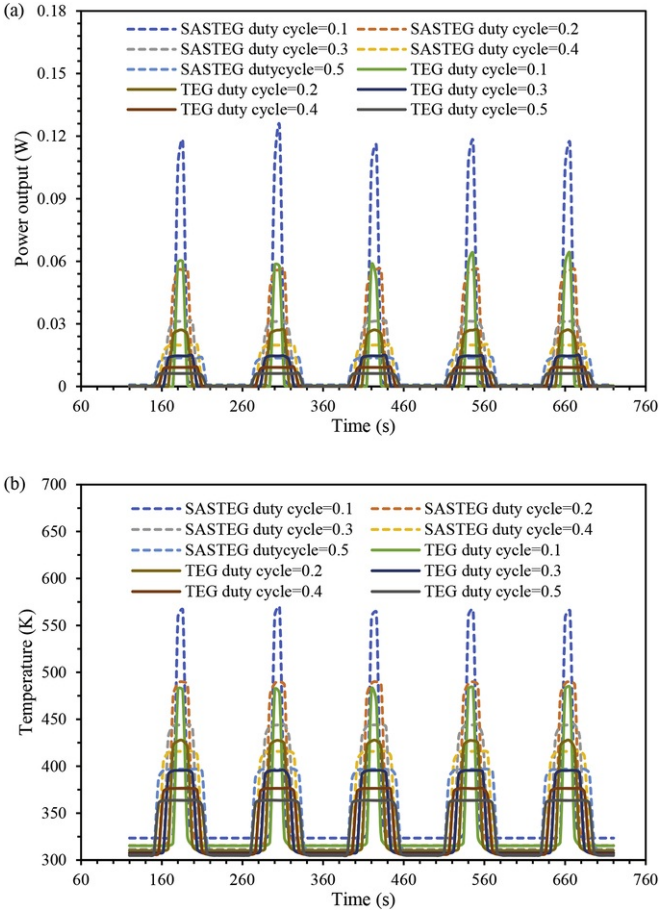

Fig. 7 Variation of optimized SASTEG and TEG (a) power output and (b) temperature with duty cycle.

alt-text: Fig. 7

4.4 Thermal stress distribution in SASTEG and TEG

Fig. 8 shows the thermal stress distribution in the segmented asymmetrical thermoelectric generator and the TEG especially, the areas with high thermal stress concentrations. The maximum von Mises stress developed in the n-type and p-type legs of the conventional TEG, SASTEG and optimized SASTEG are shown in Fig. 8a, b and c respectively. It can be seen clearly from all the figures that the maximum von Mises stress occurs at the hot surface of the thermoelectric legs and it is highly concentrated at the edges of the thermoelectric legs which are the positions most likely to crack. The lifespan of a thermoelectric generator is affected by the intensity of thermal stress developed in its legs therefore, it is important to reduce this stress. Comparing the initial SASTEG geometry in Fig. 8b to the optimized geometry in Fig. 8c, it is obvious that the maximum von Mises stress in the legs has been reduced due to the geometry optimization. Asides changing the height ratio in the SASTEG to reduce the thermal stress, increase in thermoelectric leg length can also reduce the thermal stress in a thermoelectric generator [34,49]. In addition, the use of asymmetrical legs can lead to reduced thermal stress developed in the thermoelectric generator [36].

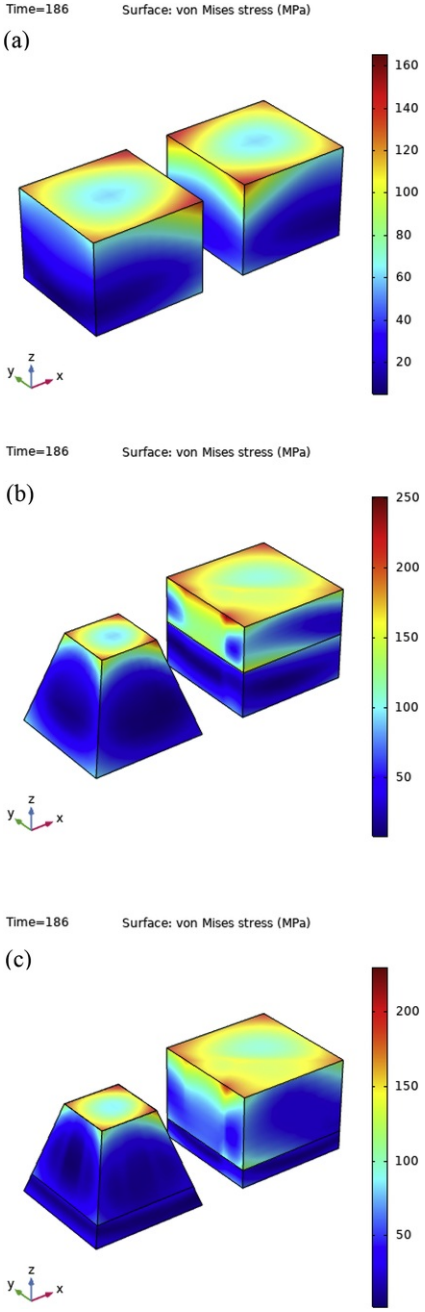

Fig. 8 Thermal stress distribution in (a) thermoelectric generator (b) segmented asymmetrical thermoelectric generator and (c) optimized SASTEG geometry.

alt-text: Fig. 8

5 Conclusion

A comprehensive numerical investigation of a segmented asymmetrical thermoelectric generator (SASTEG) and a conventional thermoelectric generator (TEG) was performed in this study. A three-dimensional model was developed and solved using finite element method in COMSOL 5.3 Multiphysics software. The thermal (temperature and thermal stress) and electrical (output voltage, current and power output) performance of the SASTEG and TEG were analysed using the numerical model under transient and steady state heating conditions. Rectangular pulsed heat input flux was applied to both devices and the temperature dependency of thermoelectric material properties was accounted for. The optimization of a thermoelectric generator by the application of pulsed heat power to a segmented asymmetrical thermoelectric generator was performed and results obtained were compared with that of the conventional symmetrical non-segmented thermoelectric generator. The focus of this study was to enhance the performance of the thermoelectric generator while also reducing the thermal stress developed in the device. Furthermore, copper and solder which display an elastoplastic behaviour were accounted for and modelled as such thus, the thermal stress predictions in the thermoelectric generator were accurate. The transient and steady state response of the SASTEG and TEG to temperature, voltage, current and power output were studied for five continuous time periods with each period lasting for 12s. In the entire study, the overall heat input under pulsed heating was equal to that of the steady state heating and the average heat flux was $60 kW \cdot m^{-2}$. The ratio of maximum input heat flux to minimum heat flux (b/a) was kept constant throughout this study and the matched load resistances for the SASTEG and TEG were also kept constant in the entire study for both the steady state heating and pulsed heating conditions in order to simplify the model. Furthermore, the asymmetrical leg was obtained by varying the cross-sectional area across the leg height.

Two stages of optimization were performed on the SASTEG to reduce its thermal stress at an enhanced electrical performance condition. In the first stage, the optimum height ratio for the p-type leg (H_p) was found and then kept constant while the n-type leg was segmented and similarly, its optimum height ratio (H_n) was also determined. Finally, the optimized SASTEG was compared to the conventional TEG and the effects of duty cycle on both devices were investigated. The major conclusions from this study are summarized as follows:

1) Rectangular pulsed heat power enhances the performance of SASTEG and TEG significantly compared to steady state heating.

2) Under transient condition, the maximum von Mises stress in the SASTEG hot side p-leg reduced by about 20.95% while that of the cold side p-leg reduced by 21.16% simply because of the optimization of the height ratio (H_p).

3) Asymmetrical leg geometry (n-type) optimization reduced the thermal stress developed in the leg by 7.45% and 39.21% for the SASTEG hot side and cold side respectively compared to the values of the symmetrical leg geometry (p-type).

4) The power output of the optimized SASTEG with optimum height ratio $H_p = H_n = 0.2$ was greater than that of the conventional TEG by 117.11%.

5) The optimized SASTEG geometry provided an enhanced electrical performance at a reduced thermal stress condition thereby increasing the SASTEG's reliability.

6) The optimum duty cycle found in this study was 0.1 for the SASTEG and TEG.

Acknowledgement

This study was sponsored by the Project of EU Marie Curie International incoming Fellowships Program (745614). The authors would also like to express our appreciation for the financial supports from EPSRC (EP/R004684/1) and Innovate UK (TSB 70507-481546) for the Newton Fund - China-UK Research and Innovation Bridges Competition 2015 Project 'A High Efficiency, Low Cost and Building Integrate-able Solar Photovoltaic/Thermal (PV/T) system for Space Heating, Hot Water and Power Supply' and DongGuan Innovation Research Team Program (No. 2014607101008).

References

[1] N. Kannan and D. Vakeesan, Solar energy for future world: - a review, *Renew. Sustain. Energy Rev.* **62**, 2016, 1092–1105, https://doi.org/10.1016/j.rser.2016.05.022.

[2] N.L. Panwar, S.C. Kaushik and S. Kothari, Role of renewable energy sources in environmental protection: a review, *Renew. Sustain. Energy Rev.* **15**, 2011, 1513–1524, https://doi.org/10.1016/j.rser.2010.11.037.

[3] T.M.O. Diallo, M. Yu, J. Zhou, X. Zhao, S. Shittu, G. Li, J. Ji and D. Hardy, Energy performance analysis of a novel solar PVT loop heat pipe employing a microchannel heat pipe evaporator and a PCM triple heat exchanger, *Energy* **167**, 2019, 866–888 https://doi.org/10.1016/j.energy.2018.10.192.

[4] K. Anoune, M. Bouya, A. Astito and A. Ben Abdellah, Sizing methods and optimization techniques for PV-wind based hybrid renewable energy system: a review, *Renew. Sustain. Energy Rev.* **93**, 2018, 652–673, https://doi.org/10.1016/j.rser.2018.05.032.

[5] S. Shittu, G. Li, Y.G. Akhlaghi, X. Ma, X. Zhao and E. Ayodele, Advancements in thermoelectric generators for enhanced hybrid photovoltaic system performance, *Renew. Sustain. Energy Rev.* **109**, 2019, 24–54,

https://doi.org/10.1016/j.rser.2019.04.023.

[6] N.S. Nazri, A. Fudholi, B. Bakhtyar, C.H. Yen, A. Ibrahim, M.H. Ruslan, S. Mat and K. Sopian, Energy economic analysis of photovoltaic–thermal-thermoelectric (PVT-TE) air collectors, *Renew. Sustain. Energy Rev.* **92**, 2018, 187–197, https://doi.org/10.1016/j.rser.2018.04.061.

[7] G. Li, S. Shittu, T.M.O. Diallo, M. Yu, X. Zhao and J. Ji, A review of solar photovoltaic-thermoelectric hybrid system for electricity generation, *Energy* **158**, 2018, 41–58, https://doi.org/10.1016/j.energy.2018.06.021.

[8] S.B. Riffat and X. Ma, Thermoelectrics: a review of present and potential applications, *Appl. Therm. Eng.* **23**, 2003, 913–935, https://doi.org/10.1016/S1359-4311(03)00012-7.

[9] D. Ji, Z. Wei, S. Mazzoni, M. Mengarelli, S. Rajoo, J. Zhao, J. Pou and A. Romagnoli, Thermoelectric generation for waste heat recovery: application of a system level design optimization approach via Taguchi method, *Energy Convers. Manag.* **172**, 2018, 507–516, https://doi.org/10.1016/j.enconman.2018.06.016.

[10] L. Francioso, C. De Pascali, I. Farella, C. Martucci, P. Cretì, P. Siciliano and A. Perrone, Flexible thermoelectric generator for wearable biometric sensors, *Proc. IEEE Sensors.* **196**, 2010, 747–750, https://doi.org/10.1109/ICSENS.2010.5690757.

[11] S.J. Kim, J.H. We and B.J. Cho, A wearable thermoelectric generator fabricated on a glass fabric, *Energy Environ. Sci.* **7**, 2014, 1959–1965, https://doi.org/10.1039/c4ee00242c.

[12] S. Qing, A. Rezania, L.A. Rosendahl and X. Gou, Design of flexible thermoelectric generator as human body sensor, *Mater. Today Proc.* **5**, 2018, 10338–10346, https://doi.org/10.1016/j.matpr.2017.12.282.

[13] F. Suarez, A. Nozariasbmarz, D. Vashaee and M.C. Öztürk, Designing thermoelectric generators for self-powered wearable electronics, *Energy Environ. Sci.* **9**, 2016, 2099–2113, https://doi.org/10.1039/c6ee00456c.

[14] S. Shittu, G. Li, X. Zhao, Y.G. Akhlaghi, X. Ma and M. Yu, Comparative study of a concentrated photovoltaic-thermoelectric system with and without fl at plate heat pipe, *Energy Convers. Manag.* **193**, 2019, 1–14, https://doi.org/10.1016/j.enconman.2019.04.055.

[15] N. Kempf and Y. Zhang, Design and optimization of automotive thermoelectric generators for maximum fuel efficiency improvement, *Energy Convers. Manag.* **121**, 2016, 224–231, https://doi.org/10.1016/j.enconman.2016.05.035.

[16] A. Marvão, P.J. Coelho and H.C. Rodrigues, Optimization of a thermoelectric generator for heavy-duty vehicles, *Energy Convers. Manag.* **179**, 2019, 178–191, https://doi.org/10.1016/j.enconman.2018.10.045.

[17] P. Fernández-Yañez, O. Armas, A. Capetillo and S. Martínez-Martínez, Thermal analysis of a thermoelectric generator for light-duty diesel engines, *Appl. Energy* **226**, 2018, 690–702, https://doi.org/10.1016/j.apenergy.2018.05.114.

[18] P. Fernández-Yáñez, O. Armas, R. Kiwan, A.G. Stefanopoulou and A.L. Boehman, A thermoelectric generator in exhaust systems of spark-ignition and compression-ignition engines. A comparison with an electric turbo-generator, *Appl. Energy* **229**, 2018, 80–87, https://doi.org/10.1016/j.apenergy.2018.07.107.

[19] D. Champier, Thermoelectric generators: a review of applications, *Energy Convers. Manag.* **140**, 2017, 167–181, https://doi.org/10.1016/j.enconman.2017.02.070.

[20] D. Madan, Z. Wang, P.K. Wright and J.W. Evans, Printed flexible thermoelectric generators for use on low levels of waste heat, *Appl. Energy* **156**, 2015, 587–592, https://doi.org/10.1016/j.apenergy.2015.07.066.

[21] K. Sornek, M. Filipowicz, M. Żołądek, R. Kot and M. Mikrut, Comparative analysis of selected thermoelectric generators operating with wood-fired stove, *Energy* **166**, 2019, 1303–1313, https://doi.org/10.1016/j.energy.2018.10.140.

[22] A. Nour Eddine, D. Chalet, X. Faure, L. Aixala and P. Chessé, Optimization and characterization of a thermoelectric generator prototype for marine engine application, *Energy* **143**, 2018, 682–695, https://doi.org/10.1016/j.energy.2017.11.018.

[23] W. He, G. Zhang, X. Zhang, J. Ji, G. Li and X. Zhao, Recent development and application of thermoelectric generator and cooler, *Appl. Energy* **143**, 2015, 1–25 https://doi.org/10.1016/j.apenergy.2014.12.075.

[24] I. Temizer and C. Ilkiliç, The performance and analysis of the thermoelectric generator system used in diesel engines, *Renew. Sustain. Energy Rev.* **63**, 2016, 141–151, https://doi.org/10.1016/j.rser.2016.04.068.

[25] M.H. Elsheikh, D.A. Shnawah, M.F.M. Sabri, S.B.M. Said, H.M. Hassan, A.M.B. Bashir and M. Mohamad, A review on thermoelectric renewable energy: principle parameters that affect their performance, *Renew. Sustain.*

Energy Rev. **30**, 2014, 337–355, https://doi.org/10.1016/j.rser.2013.10.027.

[26] M. Bittner, N. Kanas, R. Hinterding, F. Steinbach, J. Räthel, M. Schrade, K. Wiik, M.A. Einarsrud and A. Feldhoff, A comprehensive study on improved power materials for high-temperature thermoelectric generators, *J. Power Sources* **410–411**, 2019, 143–151, https://doi.org/10.1016/j.jpowsour.2018.10.076.

[27] G. Li, S. Shittu, X. Ma and X. Zhao, Comparative analysis of thermoelectric elements optimum geometry between Photovoltaic-thermoelectric and solar thermoelectric, *Energy* **171**, 2019, 599–610, https://doi.org/10.1016/j.energy.2019.01.057.

[28] S. Ferreira-Teixeira and A.M. Pereira, Geometrical optimization of a thermoelectric device: numerical simulations, *Energy Convers. Manag.* **169**, 2018, 217–227, https://doi.org/10.1016/j.enconman.2018.05.030.

[29] S. Shittu, G. Li, X. Zhao and X. Ma, Series of detail comparison and optimization of thermoelectric element geometry considering the PV effect, *Renew. Energy* **130**, 2019, 930–942 https://doi.org/10.1016/j.renene.2018.07.002.

[30] C. Hadjistassou, E. Kyriakides and J. Georgiou, Designing high efficiency segmented thermoelectric generators, *Energy Convers. Manag.* **66**, 2013, 165–172, https://doi.org/10.1016/j.enconman.2012.07.030.

[31] Y. Ge, Z. Liu, H. Sun and W. Liu, Optimal design of a segmented thermoelectric generator based on three-dimensional numerical simulation and multi-objective genetic algorithm, *Energy* **147**, 2018, 1060–1069, https://doi.org/10.1016/j.energy.2018.01.099.

[32] C. Lundgaard and O. Sigmund, Design of segmented off-diagonal thermoelectric generators with topology optimization, *Appl. Energy* **236**, 2019, 950–960, (doi:n/a).

[33] Z. Ouyang and D. Li, Design of segmented high-performance thermoelectric generators with cost in consideration, *Appl. Energy* **221**, 2018, 112–121, https://doi.org/10.1016/j.apenergy.2018.03.106.

[34] S. Fan and Y. Gao, Numerical simulation on thermoelectric and mechanical performance of annular thermoelectric generator, *Energy* **150**, 2018, 38–48, https://doi.org/10.1016/j.energy.2018.02.124.

[35] T. Ming, W. Yang, Y. Wu, Y. Xiang, X. Huang, J. Cheng, X. Li and J. Zhao, Numerical analysis on the thermal behavior of a segmented thermoelectric generator, *Int. J. Hydrogen Energy* **42**, 2017, 3521–3535, https://doi.org/10.1016/j.ijhydene.2016.11.021.

[36] A.S. Al-Merbati, B.S. Yilbas and A.Z. Sahin, Thermodynamics and thermal stress analysis of thermoelectric power generator: influence of pin geometry on device performance, *Appl. Therm. Eng.* **50**, 2013, 683–692, https://doi.org/10.1016/j.applthermaleng.2012.07.021.

[37] A. Fabián-Mijangos, G. Min and J. Alvarez-Quintana, Enhanced performance thermoelectric module having asymmetrical legs, *Energy Convers. Manag.* **148**, 2017, 1372–1381, https://doi.org/10.1016/j.enconman.2017.06.087.

[38] H.-B. Liu, J.-H. Meng, X.-D. Wang and W.-H. Chen, A new design of solar thermoelectric generator with combination of segmented materials and asymmetrical legs, *Energy Convers. Manag.* **175**, 2018, 11–20, https://doi.org/10.1016/j.enconman.2018.08.095.

[39] S. Mahmoudinezhad, A. Rezania, P.A. Cotfas, D.T. Cotfas and L.A. Rosendahl, Transient behavior of concentrated solar oxide thermoelectric generator, *Energy* **168**, 2019, 823–832, https://doi.org/10.1016/j.energy.2018.12.001.

[40] N.Q. Nguyen and K.V. Pochiraju, Behavior of thermoelectric generators exposed to transient heat sources, *Appl. Therm. Eng.* **51**, 2013, 1–9, https://doi.org/10.1016/j.applthermaleng.2012.08.050.

[41] R. Merienne, J. Lynn, E. McSweeney and S.M. O'Shaughnessy, Thermal cycling of thermoelectric generators: the effect of heating rate, *Appl. Energy* **237**, 2019, 671–681, https://doi.org/10.1016/j.apenergy.2019.01.041

[42] W.H. Chen, P.H. Wu, X.D. Wang and Y.L. Lin, Power output and efficiency of a thermoelectric generator under temperature control, *Energy Convers. Manag.* **127**, 2016, 404–415, https://doi.org/10.1016/j.enconman.2016.09.039.

[43] L. Chen and J. Lee, Effect of pulsed heat power on the thermal and electrical performances of a thermoelectric generator, *Appl. Energy* **150**, 2015, 138–149, https://doi.org/10.1016/j.apenergy.2015.04.009.

[44] S. Asaadi, S. Khalilarya and S. Jafarmadar, Numerical study on the thermal and electrical performance of an annular thermoelectric generator under pulsed heat power with different types of input functions, *Energy Convers. Manag.* **167**, 2018, 102–112, https://doi.org/10.1016/j.enconman.2018.04.085.

[45] Z. Ouyang and D. Li, Modelling of segmented high-performance thermoelectric generators with effects of thermal radiation, electrical and thermal contact resistances, *Sci. Rep.* **6**, 2016, 1–12, https://doi.org/10.1038/srep24123.

[46] D.M. Rowe, Thermoelectric Handbook: Macro to Nano, 2006, CRC Press, Taylor & Francis Group.

[47] G. Li, Q. An, W. Li, W.A. Goddard, P. Zhai, Q. Zhang and G.J. Snyder, Brittle failure mechanism in thermoelectric skutterudite CoSb3, *Chem. Mater.* **27**, 2015, 6329–6336, https://doi.org/10.1021/acs.chemmater.5b02268.

[48] B.S. Yilbas, S.S. Akhtar and A.Z. Sahin, Thermal and stress analyses in thermoelectric generator with tapered and rectangular pin configurations, *Energy* **114**, 2016, 52–63, https://doi.org/10.1016/j.energy.2016.07.168.

[49] S. Shittu, G. Li, X. Zhao, X. Ma, Y.G. Akhlaghi and E. Ayodele, High performance and thermal stress analysis of a segmented annular thermoelectric generator, *Energy Convers. Manag.* **184**, 2019, 180–193, https://doi.org/10.1016/j.enconman.2019.01.064.

[50] Z.-G. Shen, X. Liu, S. Chen, S.-Y. Wu, L. Xiao and Z.-X. Chen, Theoretical analysis on a segmented annular thermoelectric generator, *Energy* **157**, 2018, 297–313, https://doi.org/10.1016/j.energy.2018.05.163.

[51] J.-L. Gao, Q.-G. Du, X.-D. Zhang and X.-Q. Jiang, Thermal stress analysis and structure parameter selection for a Bi2Te3-based thermoelectric module, *J. Electron. Mater.* **40**, 2011, 884–888, https://doi.org/10.1007/s11664-011-1611-3.

[52] X. Yang, P. Zhai, L. Liu and Q. Zhang, Thermodynamic and mechanical properties of crystalline CoSb(3): a molecular dynamics simulation study, *J. Appl. Phys.* **109**, 2011, 123517/1–123517/6, https://doi.org/10.1063/1.3598116.

[53] T. Caillat, A. Borshchevsky and J.P. Fleurial, Properties of single crystalline semiconducting CoSb3, *J. Appl. Phys.* **80**, 1996, 4442–4449, https://doi.org/10.1063/1.363405.

[54] Q. Ma, H. Fang and M. Zhang, Theoretical analysis and design optimization of thermoelectric generator, *Appl. Therm. Eng.* **127**, 2017, 758–764, https://doi.org/10.1016/j.applthermaleng.2017.08.056.

[55] G. Li, X. Zhao, Y. Jin, X. Chen, J. Ji and S. Shittu, Performance analysis and discussion on the thermoelectric element footprint for PV–TE maximum power generation, *J. Electron. Mater.* **47**, 2018, 5344–5351, https://doi.org/10.1007/s11664-018-6421-4.

[56] H. Sun, Y. Ge, W. Liu and Z. Liu, Geometric optimization of two-stage thermoelectric generator using genetic algorithms and thermodynamic analysis, *Energy* **171**, 2019, 37–48, https://doi.org/10.1016/j.energy.2019.01.003.

[57] G. Li, K. Zhou, Z. Song, X. Zhao and J. Ji, Inconsistent phenomenon of thermoelectric load resistance for photovoltaic–thermoelectric module, *Energy Convers. Manag.* **161**, 2018, 155–161 https://doi.org/10.1016/j.enconman.2018.01.079.

[58] X. Yu, X. Lu, Q. Wang, Y. Chen and T. Ma, Parametric study of thermoelectric power generators under large temperature difference conditions, *Appl. Therm. Eng.* **144**, 2018, 647–657, https://doi.org/10.1016/j.applthermaleng.2018.08.079.

[59] G. Li, X. Zhao and J. Ji, Conceptual development of a novel photovoltaic-thermoelectric system and preliminary economic analysis, *Energy Convers. Manag.* **126**, 2016, 935–943, https://doi.org/10.1016/j.enconman.2016.08.074.

[60] G. Li, G. Zhang, W. He, J. Ji, S. Lv, X. Chen and H. Chen, Performance analysis on a solar concentrating thermoelectric generator using the micro-channel heat pipe array, *Energy Convers. Manag.* **112**, 2016, 191–198 https://doi.org/10.1016/j.enconman.2016.01.025.

[61] G. Li, W. Feng, Y. Jin, X. Chen and J. Ji, Discussion on the solar concentrating thermoelectric generation using micro-channel heat pipe array, *Heat Mass Transf.* **53**, 2017, 3249–3256, https://doi.org/10.1007/s00231-017-2026-3.

[62] G. Li, J. Ji, G. Zhang, W. He, X. Chen and H. Chen, Performance analysis on a novel micro-channel heat pipe evacuated tube solar collector-incorporated thermoelectric generation, *Int. J. Energy Res.* **40**, 2016, 2117–2127, https://doi.org/10.1002/er.3589.

[63] G. Shu, X. Ma, H. Tian, H. Yang, T. Chen and X. Li, Configuration optimization of the segmented modules in an exhaust-based thermoelectric generator for engine waste heat recovery, *Energy* **160**, 2018, 612–624, https://doi.org/10.1016/j.energy.2018.06.175.

[64] H. Tian, X. Sun, Q. Jia, X. Liang, G. Shu and X. Wang, Comparison and parameter optimization of a segmented thermoelectric generator by using the high temperature exhaust of a diesel engine, *Energy* **84**, 2015, 121–130, https://doi.org/10.1016/j.energy.2015.02.063.

[65] O. Yamashita, H. Odahara and K. Satou, Energy conversion efficiency of a thermoelectric generator under the periodically alternating temperature gradients, *J. Appl. Phys.* **101**, 2007, https://doi.org/10.1063/1.2425005.

[66] O. Yamashita, H. Odahara and T. Ochi, Energy conversion efficiency of a welded Cu/Bi-Te/Cu composite under periodically alternating temperature gradients, *Appl. Energy* **86**, 2009, 273–283, https://doi.org/10.1016/j.apenergy.2008.04.014.

Nomenclature

H: Leg height, mm

H_p: Height ratio of p-type leg

H_n: Height ratio of n-type leg

D: Ceramic depth, mm

W_{le}: Leg width, mm

W_{ce}: Ceramic width

t^{ρ} : Heating time

τ : Period

q": Input heat flux

Q_{in}: Input flux power, W/m^2

Q_{out}: Output flux power, W/m^2

R_L: Load resistance, Ω

P_{out}: Power output, W

C_P : Specific heat capacity, J/kg/K

T: Temperature, K

E: Young's modulus, GPa

Z: Figure of merit

Greek symbols

α : Seebeck coefficient, $V{\cdot}K^{-1}$

σ : Electrical conductivity, $S{\cdot}m^{-1}$

κ : Thermal conductivity, $W{\cdot}m^{-1}{\cdot}K^{-1}$

ρ_d : Density, $kg{\cdot}m^{-3}$

ρ : Electrical resistivity, $\Omega{\cdot}m$

Abbreviations

SASTEG: Segmented asymmetrical thermoelectric generator

STEG: Segmented thermoelectric generator

TEG: Thermoelectric generator

Bi_2Te_3: Bismuth telluride

$CoSb_3$: Cobalt Antimony

Subscripts

c: Cold side

h: Hot side

Highlights

- A thermoelectric generator with segmented materials and asymmetrical leg is studied.
- Rectangular pulsed heating and steady state heating are applied to the TEG.
- Geometry optimization is done to reduce thermal stress and enhance power output.
- Comparison is made between the new TEG design and conventional TEG design.

Queries and Answers

Query: Please confirm that the provided email “Guiqiang.Li@hull.ac.uk” is the correct address for official communication, else provide an alternate e-mail address to replace the existing one, because private e-mail addresses should not be used in articles as the address for communication.
Answer: Yes

Query: Have we correctly interpreted the following funding source(s) and country names you cited in your article: TSB, UK; EPSRC, UK; Marie Curie International incoming Fellowships Program, UK; UK Research and Innovation Bridges Competition, UK; DongGuan Innovation Research Team Program, China?
Answer: Yes

Query: Please confirm that given names and surnames have been identified correctly and are presented in the desired order and please carefully verify the spelling of all authors’ names.
Answer: Yes

Query: Your article is registered as a regular item and is being processed for inclusion in a regular issue of the journal. If this is NOT correct and your article belongs to a Special Issue/Collection please contact s.turner.1@elsevier.com immediately prior to returning your corrections.
Answer: Yes